Research Article | Vol. 26, No. 4 | 19 Feb 2018 | OPTICS EXPRESS 3801

Optics EXPRESS

Incubation during laser ablation with bursts of femtosecond pulses with picosecond delays

CATERINA GAUDIUSO,[1,2,*] GIUSEPPE GIANNUZZI,[1,2] ANNALISA VOLPE,[1] PIETRO MARIO LUGARÀ,[1,2] ISABELLE CHOQUET,[3] AND ANTONIO ANCONA[1,3]

[1]*Istituto di Fotonica e Nanotecnologie (IFN)-CNR U.O.S. Bari, via Amendola 173, I-70126 Bari, Italy*
[2]*Università degli Studi di Bari, Dipartimento Interuniversitario di Fisica, via Amendola 173, I-70126 Bari, Italy*
[3]*University West, Department of Engineering Sciences, 461 80 Trollhättan, Sweden*
[*]*caterina.gaudiuso@uniba.it*

Abstract: We report on an experimental investigation of the incubation effect during irradiation of stainless steel with bursts of ultrashort laser pulses. A series of birefringent crystals was used to split the pristine 650-fs pulses into bursts of up to 32 sub-pulses with time separations of 1.5 ps and 3 ps, respectively. The number of selected bursts was varied between 50 and 1600. The threshold fluence was measured in case of Burst Mode (BM) processing depending on the burst features, i.e. the number of sub-pulses and their separation time, and on the number of bursts. We found as many values of threshold fluence as the combinations of the number of bursts and of sub-pulses constituting the bursts set to give the same total number of impinging sub-pulses. However, existing incubation models developed for Normal Pulse Mode (NPM) return, for a given number of impinging pulses, a constant value of threshold fluence. Therefore, a dependence of the incubation coefficient with the burst features was hypothesized and experimentally investigated. Numerical solutions of the Two Temperature Model (TTM) in case of irradiation with single bursts of up to 4 sub-pulses have been performed to interpret the experimental results.

© 2018 Optical Society of America under the terms of the OSA Open Access Publishing Agreement

OCIS codes: (350.3390) Laser materials processing; (320.7090) Ultrafast lasers; (140.3510) Lasers, fiber; (320.5550) Pulses; (160.3900) Metals; (320.7130) Ultrafast processes in condensed matter, including semiconductors; (120.6810) Thermal effects; (140.3330) Laser damage; (140.3390) Laser materials processing.

References and links

1. J.-P. Negel, A. Loescher, A. Voss, D. Bauer, D. Sutter, A. Killi, M. A. Ahmed, and T. Graf, "Ultrafast thin-disk multipass laser amplifier delivering 1.4 kW (4.7 mJ, 1030 nm) average power converted to 820 W at 515 nm and 234 W at 343 nm," Opt. Express **23**(16), 21064–21077 (2015).
2. E. Mottay, X. Liu, H. Zhang, E. Mazur, R. Sanatinia, and W. Pfleging, "Industrial applications of ultrafast laser processing," MRS Bull. **41**(12), 984–992 (2016).
3. T. Eidam, S. Hanf, E. Seise, T. V. Andersen, T. Gabler, C. Wirth, T. Schreiber, J. Limpert, and A. Tünnermann, "Femtosecond fiber CPA system emitting 830 W average output power," Opt. Lett. **35**(2), 94–96 (2010).
4. M. Müller, M. Kienel, A. Klenke, T. Gottschall, E. Shestaev, M. Plötner, J. Limpert, and A. Tünnermann, "1 kW 1 mJ eight-channel ultrafast fiber laser," Opt. Lett. **41**(15), 3439–3442 (2016).
5. R. Jung, J. Tümmler, T. Nubbemeyer, and I. Will, "Thin-disk ring amplifier for high pulse energy," Opt. Express **24**(5), 4375–4381 (2016).
6. V. S. Belyaev, A. P. Matafonov, V. I. Vinogradov, V. P. Krainov, V. S. Lisitsa, A. S. Roussetski, G. N. Ignatyev, and V. P. Andrianov, "Observation of neutronless fusion reactions in picosecond laser plasmas," Phys. Rev. E Stat. Nonlin. Soft Matter Phys. **72**(2), 026406 (2005).
7. F. Bauer, A. Michalowski, T. Kiedrowski, and S. Nolte, "Heat accumulation in ultra-short pulsed scanning laser ablation of metals," Opt. Express **23**(2), 1035–1043 (2015).
8. S. Eaton, H. Zhang, P. Herman, F. Yoshino, L. Shah, J. Bovatsek, and A. Arai, "Heat accumulation effects in femtosecond laser-written waveguides with variable repetition rate," Opt. Express **13**(12), 4708–4716 (2005).
9. R. Weber, T. Graf, P. Berger, V. Onuseit, M. Wiedenmann, C. Freitag, and A. Feuer, "Heat accumulation during pulsed laser materials processing," Opt. Express **22**(9), 11312–11324 (2014).
10. A. Ancona, F. Röser, K. Rademaker, J. Limpert, S. Nolte, and A. Tünnermann, "High speed laser drilling of metals using a high repetition rate, high average power ultrafast fiber CPA system," Opt. Express **16**(12), 8958–8968 (2008).

#309616 https://doi.org/10.1364/OE.26.003801
Journal © 2018 Received 20 Oct 2017; revised 9 Dec 2017; accepted 19 Dec 2017; published 5 Feb 2018

Optics EXPRESS

11. R. R. Gattass, L. R. Cerami, and E. Mazur, "Micromachining of bulk glass with bursts of femtosecond laser pulses at variable repetition rates," Opt. Express **14**(12), 5279–5284 (2006).
12. B. Dromey, M. Zepf, M. Landreman, K. O'keeffe, T. Robinson, and S. M. Hooker, "Generation of a train of ultrashort pulses from a compact birefringent crystal array," Appl. Opt. **46**(22), 5142–5146 (2007).
13. S. Zhou, D. Ouzounov, H. Li, I. Bazarov, B. Dunham, C. Sinclair, and F. W. Wise, "Efficient temporal shaping of ultrashort pulses with birefringent crystals," Appl. Opt. **46**(35), 8488–8492 (2007).
14. A. M. Weiner, "Femtosecond pulse shaping using spatial light modulators," Rev. Sci. Instrum. **71**(5), 1929–1960 (2000).
15. R. Stoian, S. Winkler, M. Hildebrand, M. Boyle, A. Thoss, M. Spyridaki, E. Koudoumas, N. M. Bulgakova, A. Rosenfeld, P. Tzanetakis, C. Fotakis, and I. V. Hertel, "Temporal Pulse Shaping and Optimization in Ultrafast Laser Ablation of Materials," Appl. Phys. Lett. **780**, 183–194 (2003).
16. L. Englert, B. Rethfeld, L. Haag, M. Wollenhaupt, C. Sarpe-Tudoran, and T. Baumert, "Control of ionization processes in high band gap materials via tailored femtosecond pulses," Opt. Express **15**(26), 17855–17862 (2007).
17. J. Huang, Y. Zhang, J. K. Chen, and M. Yang, "Modeling of ultrafast phase change processes in a thin metel film irradiated by femtosecond laser pulse trains," J. Heat Transfer **133**(3), 031003 (2011).
18. R. Knappe, H. Haloui, A. Seifert, A. Weis, and A. Nebel, "Scaling ablation rates for picosecond lasers using burst micromachining," Proc. SPIE **7585**, 75850H (2010).
19. O. Andrusyak, M. Bubelnik, J. Mares, T. McGovern, and C. W. Siders, "Single-pulse and burst-mode ablation of gold films measured by quartz crystal microbalance," Proc. SPIE **5647**, 61–71 (2005).
20. B. Neuenschwander, T. Kramer, B. Lauer, and B. Jaeggi, "Burst mode with ps- and fs-pulses: Influence on the removal rate, surface quality and heat accumulation," Proc. SPIE **9350**, 93500U (2015).
21. C. Gaudiuso, H. Kämmer, F. Dreisow, A. Ancona, A. Tünnermann, and S. Nolte, "Ablation of silicon with bursts of femtosecond laser pulses," Proc. SPIE **9041**, 974017 (2016).
22. W. Hu, Y. C. Shin, and G. King, "Modeling of multi-burst mode pico-second laser ablation for improved material removal rate," Appl. Phys., A Mater. Sci. Process. **98**(2), 407–415 (2009).
23. H. Kämmer, F. Dreisow, A. Tünnermann, and S. Nolte, "Analysis of the hole shape evolution in fs-pulse percussion drilling with bursts," Proc. SPIE **9740**, 974012 (2016).
24. Y. Jee, M. F. Becker, and R. M. Walser, "Laser-induced damage on single-crystal metal surfaces," J. Opt. Soc. Am. B **5**(3), 648–659 (1988).
25. C. S. R. Nathala, A. Ajami, W. Husinsky, B. Farooq, S. I. Kudryashov, A. Daskalova, I. Bliznakova, and A. Assion, "Ultrashort laser pulse ablation of copper, silicon and gelatin: effect of the pulse duration on the ablation thresholds and the incubation coefficients," Appl. Phys., A Mater. Sci. Process. **122**(107), 9625–9631 (2016).
26. P. T. Mannion, J. Magee, E. Coyne, G. M. O'Connor, and T. J. Glynn, "The effect of damage accumulation behaviour on ablation thresholds and damage morphology in ultrafast laser micro-machining of common metals in air," Appl. Surf. Sci. **233**(1–4), 275–287 (2004).
27. J. Bonse, S. Baudach, J. Krüger, W. Kautek, and M. Lenzner, "Femtosecond laser ablation of silicon-modification thresholds and morphology," Appl. Phys., A Mater. Sci. Process. **74**(1), 19–25 (2002).
28. S. Baudach, J. Bonse, J. Krüger, and W. Kautek, "Ultrashort pulse laser ablation of polycarbonate and polymethylmethacrylate," Appl. Surf. Sci. **154–155**(1–4), 555–560 (2000).
29. D. Gómez and I. Goenaga, "On the incubation effect on two thermoplastics when irradiated with ultrashort laser pulses: broadening effects when machining microchannels," Appl. Surf. Sci. **253**(4), 2230–2236 (2006).
30. L. M. Machado, R. E. Samad, W. de Rossi, and N. D. Vieira Junior, "D-Scan measurement of ablation threshold incubation effects for ultrashort laser pulses," Opt. Express **20**(4), 4114–4123 (2012).
31. F. Di Niso, C. Gaudiuso, T. Sibillano, F. P. Mezzapesa, A. Ancona, and P. M. Lugarà, "Role of heat accumulation on the incubation effect in multi-shot laser ablation of stainless steel at high repetition rates," Opt. Express **22**(10), 12200–12210 (2014).
32. D. Ashkenasi, M. Lorenz, R. Stoian, and A. Rosenfeld, "Surface damage threshold and structuring of dielectrics using femtosecond laser pulses: the role of incubation," Appl. Surf. Sci. **150**(1–4), 101–106 (1999).
33. Z. Sun, M. Lenzner, and W. Rudolph, "Generic incubation law for laser damage and ablation threshold," J. Appl. Phys. **117**(7), 073102 (2015).
34. D. Breitling, A. Ruf, and F. Dausinger, "Fundamental aspects in machining of metals with short and ultrashort laser pulses," Proc. SPIE **5339**, 49–63 (2004).
35. E. Majchrzak and J. Dziatkiewicz, "Application of the two-temperature model for a numerical study of multiple laser pulses interactions with thin metal films," Sci. Res. Institute Mathematics Computer Sci. **11**(2), 63–70 (2012).
36. S. I. Anisimov, B. L. Kapeliovich, and T. L. Perelman, "Electron emission from metal surfaces exposed to ultrashort laser pulses," Zhurmal Eksperimental'noi I Teoreticheskoi Fiziki, **66**, 776–781 (1974).
37. Z. Lin, L. V. Zhigilei, and V. Celli, "Electron-phonon coupling and electron heat capacity of metals under conditions of strong electron-phonon nonequilibrium," Phys. Rev. B **77**(075133), 1–17 (2008).
38. J. K. Chen and J. E. Beraun, "Numerical study of ultrashort laser pulse interactions with metal films," Numer. Heat Tr. A Appl. **40**, 1–20 (2001).
39. R. S. Graves, T. G. Kollie, D. L. McElroy, and K. E. Gilchrist, "The Thermal Conductivity of AISI 304L Stainless Steel," Int. J. Thermophys. **12**(2), 409–415 (1991).

Optics EXPRESS

40. M. Spittel and T. Spittel, (auth.), H. Warlimont (eds.), and L. -Börnstein - Group VIII Advanced Materials and Technologies 2C1: Advanced Materials and Technologies Metal Forming Data of Ferrous Alloys - deformation behaviour [1 ed.], Springer-Verlag Berlin Heidelberg, 2009.
41. E. Bevillon, J.-P. Colombier, B. Dutta, and R. Stoian, "Ab Initio Nonequilibrium Thermodynamic and Transport Properties of Ultrafast Laser Irradiated 316L Stainless Steel," J. Phys. Chem. C **119**(21), 11438–11446 (2015).
42. K. Salonitis, A. Stournaras, G. Tsoukantas, P. Stavropoulos, and G. Chryssolouris, "A theoretical and experimental investigation on limitations of pulsed laser drilling," J. Mater. Process. Technol. **183**(1), 96–103 (2007).
43. R. Le Harzic, D. Breitling, M. Weikert, S. Sommer, C. Föhl, S. Valette, C. Donnet, E. Audouard, and F. Dausinger, "Pulse width and energy influence on laser micromachining of metals in a range of 100 fs to 5 ps," Appl. Surf. Sci. **249**(1-4), 322–331 (2005).
44. J. M. Liu, "Simple technique for measurements of pulsed Gaussian-beam spot sizes," Opt. Lett. **7**(5), 196–198 (1982).
45. B. Neuenschwander, B. Jaeggi, M. Schmid, A. Dommann, A. Neels, T. Bandi, and G. Hennig, "Factors controlling the incubation in the application of ps laser pulses on copper and iron surfaces," Proc. SPIE **8607**, 86070D (2013).

1. Introduction

The increasing demand for high-throughput industrial use of ultrafast laser sources has driven tremendous progress in the development of high average power and high repetition rate femtosecond and picosecond laser sources. Nowadays, industrial ultrashort pulsed lasers are commercially available with average powers in the range of 100 W, pulse energies up to 400 µJ and repetition rates from several hundred KHz up to several MHz [1–3]. In addition, ultrafast laser sources with average powers of more than 1 kW and/or pulse energies up to the Joule level have been demonstrated on a laboratory scale [4-5]. New potential applications of such recently available laser technology are under investigation [6]. As regards possible exploitation in high-precision manufacturing, the expected advantage in terms of higher productivity is counterbalanced by other drawbacks such as heat accumulation. It occurs typically at repetition rates above several hundred kilohertz. Then, the time separation between consecutive pulses is too short for the fraction of laser energy released onto the target in the form of heat to diffuse out of the irradiated volume [7–9]. Pulse after pulse the target temperature increases until the surroundings of the ablated region undergo irreversible thermal damage, such as cracks or melting, which are detrimental to the quality and precision of the manufacturing process [10]. Therefore, the development of high-speed beam handling technologies, as well as optical components able to withstand laser beams of such high intensity, is becoming of paramount importance.

A possible method to overcome the limitations due to heat accumulation at high repetition rates is to use groups (or bursts) of several ultrashort laser pulses, so called Burst Mode (BM) processing. Bursts can be obtained by grouping together sequences of a few to a few tens of pulses [11], splitting each laser pulse into sub-pulses [12,13] or using Spatial Light Modulators (SLM) [14–16]. The intra-burst pulse-to-pulse time separations are of the same order of magnitude or shorter than the laser source repetition rate, typically from a few tens of nanoseconds [17,18] to a few microseconds [11]. The expected advantage from BM processing is a reduced heat load and, consequently, reduced stress and thermal damage during the manufacturing processes. In case of pulse splitting, the sub-pulses peak intensity is lower than the pristine pulse, which has been shown to prevent plasma formation and the rise of screening effects [19]. Although several experimental investigations have been performed on laser milling [18,20] and drilling [21–23] with bursts of ultrashort pulses, researchers have yet to gain a thorough understanding of the laser-matter interaction mechanisms during BM processing. For instance, a phenomenon that has attracted the interest of many researchers is that during BM processing the ablation threshold is lowered due to an effect called "incubation" [24].

A better understanding of the physical mechanism behind incubation could open the possibility to enhance the volume ablation rate by using suitable bursts of pulses depending on the material to be ablated. On the other hand, if incubation is responsible for a decrease of

Optics EXPRESS

the beam steering optics damage threshold, this could represent a severe problem for exploitation of BM processing. For this reason, it is very important to study incubation and threshold effects during laser ablation with bursts of ultrashort pulses.

First studies on incubation have been performed by irradiating steel targets with trains of *N* laser pulses [24]. The trend of the ablation threshold depending on the number of applied pulses was interpolated by a power law, which introduced an incubation coefficient *S*. Typical values of *S* between 0 and 1 were found, thus indicating a decrease of the threshold fluence with *N* due to incubation. Similar results were found for other metals [25,26], as well as semiconductors [27] and dielectrics [28–30]. Di Niso et al. [31] observed that increasing the number *N* of applied pulses above a certain value does not lead to a further reduction of the damage threshold. Therefore, they introduced a saturation value of the threshold fluence for infinite number of pulses, as it was also proposed by other groups in case of multi-pulse laser ablation of dielectrics [32]. Incubation is often ascribed to a damage accumulation mechanism, which is considered to be responsible for the lowering of the damage threshold pulse after pulse. Nonetheless, the physics of such an effect is not completely understood, yet. Sun et al. [33] have proposed that the material absorption of the laser radiation changes according to the laser fluence and in case of multi-pulse irradiation. Studying incubation during BM processing would be helpful to better understand the physical mechanism behind this effect.

So far, most experimental data available on BM processing are limited to the case of bursts of pulses with intra-burst delays in the nanosecond range [17,18,20]. Generation and exploitation of bursts with picosecond time separations between sub-pulses is almost unexplored. Investigating laser ablation of metals with bursts in the picosecond time domain would be very interesting to understand the physics of ultrafast laser-matter interaction and incubation, because the transfer of the absorbed energy from the electronic subsystem to the lattice takes place just on this time-scale [34].

In this work, we have studied incubation during laser ablation with bursts of 650 fs pulses at a wavelength of 1030 nm with intra-burst time separation of 1.5 ps and 3 ps. The ablation threshold obtained in BM processing as well as in Normal Pulse Mode (NPM) were determined and compared, keeping the laser repetition rate at 100 kHz. In particular, we aimed at investigating whether the burst features, i.e. the number of sub-pulses and the time delay, influence the ablation threshold and the incubation effect. The experimental data were interpreted based on the results of numerical simulations solving the Two Temperature Model [35] and calculating the temporal and spatial evolution of the lattice temperature after laser irradiation with single pulse, two and four pulses with 1.5 and 3 ps time delays, respectively.

2. Experimental set-up

The ultrafast laser source used for this study is a high-average-power, high-repetition-rate fiber chirped pulse amplification (CPA) system (mod. Sci-series) from Active Fiber Systems GmbH. It delivers a linearly polarized laser beam with Gaussian profile ($M^2 \sim 1.25$) at a wavelength of 1030 nm, with tunable pulse duration in the range 650 fs – 20 ps. The maximum achievable pulse energy and average laser power are 100 μJ and 50 Watt, respectively, in a tunable range of repetition rates from 50 kHz to 10 MHz. An external acousto-optic modulator allows picking from single to any desired number *N* of pulses at the selected repetition rate. In this work, the laser has been operated with the shortest pulse duration of 650 fs and at a fixed repetition rate of 100 kHz. Bursts have been generated by using an array of five birefringent calcite crystals which split the linearly polarized 650 fs laser pulses exiting from the laser source into *n* sub-pulses having the same pulse duration of the pristine pulses and equal fractioned energy. The number *n* depends on how the optical axes of the crystals are oriented with respect to the polarization of the incident pulses. By finely adjusting the orientation of each crystal of the array, it is possible to change the number

Optics EXPRESS

of sub-pulses in the burst, from 2 up to 32. More details on the burst generator set-up can be found in [12,13].

Experiments consisted in producing several craters by laser ablation on polished stainless steel (AISI304) targets either by focusing trains of undivided laser pulses of energy E_p in NPM or by employing bursts with equivalent total amount of energy E_b in BM. The laser beam was focused using a 100-mm focal length plano-convex lens at normal incidence to the targets surface. Samples were placed on the lens focal plane and translated through a motorized XY linear stage. Ablation was performed in ambient air without any gas shielding.

Bursts with different number of sub-pulses (n = 2, 4, 8, 16 and 32), two time separations Δt between sub-pulses (1.5 ps and 3 ps) and variable burst energy E_b in the range 5-25 μJ, were used. The number N of pulses in NPM or, equivalently, the number of bursts in BM was also varied in the range from 50 to 1600. Table 1 reports a summary of the set of parameters used for ablation experiments.

Table 1. Summary of investigated working parameters in BM.

Number of sub-pulses in the burst, n	2	4	8	16	32
Time separation between sub-pulses, Δt	1.5 ps 3 ps	1.5 ps 3 ps	1.5 ps 3 ps	1.5 ps 3 ps	1.5 ps
Burst energy, E_b	5 – 7.5 – 10 – 12.5 – 15 – 20 – 25 μJ				
Number of bursts, N	50 – 100 – 200 – 400 – 800 – 1600				

After ablation, in order to estimate the ablation threshold for each process condition, the crater diameters were measured with an optical microscope Nikon Eclipse ME600. Five replicas of each experimental condition have been performed for averaging the results.

3. Numerical model

The experimental measurements were supplemented with numerical simulations to calculate the temporal and spatial evolution of the lattice temperature during the laser heat treatment process. An objective is to evaluate the time and the laser energy needed for the lattice to reach the melting temperature. For ultrashort laser pulses, thermal non-equilibrium between metal electrons and lattice is known to occur [36]. A two-step heating model for metals under conditions of strong electron-phonon non-equilibrium was thus employed [37,38]. The model consists of two energy conservation equations expressed in one-space dimension

$$\partial_t\left(C_e T_e\right) = -\partial_x\left(\lambda_e \partial_x T_e\right) - G\left(T_e - T_l\right) + Q, \tag{1}$$

$$\partial_t\left(C_l T_l\right) = -\partial_x\left(\lambda_l \partial_x T_l\right) + G\left(T_e - T_l\right), \tag{2}$$

which govern the electron temperature, $T_e = T_e(x,t)$, and the lattice temperature, $T_l = T_l(x,t)$. $C_e = C_e(T_e)$ and C_l are the volumetric specific heats, $\lambda_e = \lambda_e(T_e)$ and λ_l the thermal conductivities; the subscripts e and l denote electron and lattice, respectively. $G = G(T_e)$ is the electron-phonon coupling factor, and $Q = Q(x,t)$ the heat source term related to laser power density input. The lattice thermodynamic properties were assumed constant and set to C_l = 4.1496 × 10^6 J K^{-1} m^{-3} and λ_l = 18 W K^{-1} m^{-1} [39,40]. The electron thermodynamic properties were expressed as functions of the electron temperature

$$C_e = \left[28.02 + 9.29\ln(T_e \times 10^{-4} + 0.03)\right] \times 10^5 \quad , \tag{3}$$

and

Optics EXPRESS

$$\lambda_e = \left[0.535\left(T_e \times 10^{-4}\right) - 0.004\right] \times 10^3 \ , \tag{4}$$

where C_e is in $J\,K^{-1}\,m^{-3}$, λ_e in $W\,K^{-1}\,m^{-1}$, and T_e in K. Equation (3) and (4) were obtained fitting analytic expressions to the experimental data provided in [41] for stainless steel. The electron-phonon coupling factor was expressed as an analytic function of the electron temperature by fitting the experimental data in [40],

$$G = \left[28.68 + \frac{24.25}{1 + \exp\left(\dfrac{T_e \times 10^{-4} - 1.27}{0.23}\right)}\right] \times 10^{17} \quad . \tag{5}$$

In Eq. (5), G is in $W\,K^{-1}\,m^{-3}$ and T_e is in K. The two-step heating model (1)-(5) was implemented in the open source computational software OpenFOAM®. It should be noticed the model is valid when $T_l \le T_m$ where T_m denotes the melting temperature, and it becomes oversimplified when T_l exceeds T_m since the energy sink term of fusion enthalpy is not taken into account in (2). In addition, the optical properties, i.e. absorption length and reflectivity, of the solid material are considered constant during irradiation.

4. Results and discussion

4.1 Numerical simulations

The model described in section 3 was applied to calculate the electron and lattice temperatures as functions of time and position through the thickness of a sample. The laser power density source term was given by

$$Q = I\left(t\right)\left(1 - R\right)\alpha\, exp\left(-\alpha\, x\right), \tag{6}$$

where R is the reflectivity of the irradiated surface, and α^{-1} the optical penetration depth. These parameters were set to $R = 0.9$ and $\alpha = 51 \times 10^4$ cm^{-1} [42,43]. The laser beam time profile $I = I(t)$ was given by

$$I = \sqrt{\frac{\beta}{\pi}}\ \frac{I_0}{n} \sum_{i=0}^{n-1} exp\left[-\beta \frac{\left(t - \left(i\,\Delta t + t_o\right)\right)^2}{\tau^2}\right]$$

where $\beta = 4\ln 2$, $I_0 = F_0 / \tau$, τ denotes the pulse duration, and t_0 is the time at which the laser source is switched on. F_0 is the peak laser fluence defined as a function of the pulse energy E and the laser spot radius w on the sample surface. These parameters were set to $\tau = 650$ fs, $w = 21.5$ μm, $E = 5$ μJ, and $t_0 = 5$ ps. Three cases were calculated: single pulse $(n = 1)$, two sub-pulses $(n = 2)$ and four sub-pulses ($n = 4$).

Optics EXPRESS

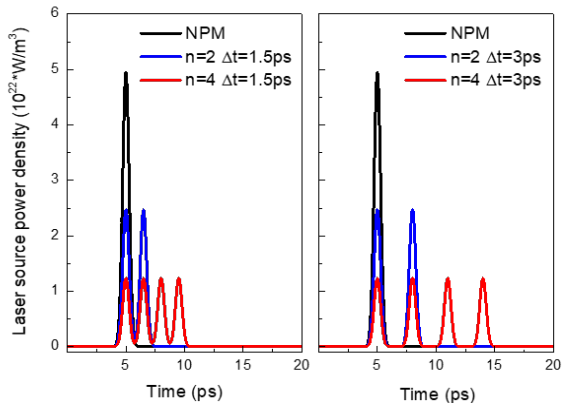

Fig. 1. Laser power density as a function of time calculated on the top surface of the sample (i.e. in $x = 0$) in case of constant burst energy. On the left: NPM and BM with time separation of 1.5ps and 2 and 4 sub-pulses; on the right: NPM and BM with time separation of 3ps and 2 and 4 sub-pulses.

The calculations were done for two values of the time between sub-pulses, $\Delta t = 1.5$ ps and $\Delta t = 3$ ps. The laser power density on the top surface of the sample (i.e. in $x = 0$) is plotted as a function of time in Fig. 1 for these different combinations of *n* and Δ*t*. As clearly shown in Fig. 1, the numerical simulations were carried out by keeping fixed the total laser intensity impinging on the sample (i.e. the laser energy heat source), both in NPM and BM.

It was assumed that heat transfer to the surroundings is negligible during the short time interval of interest in this study (the time needed for the lattice to reach melting). Sample cooling by natural convection and radiation were thus neglected and Neumann boundary conditions with zero gradient set in $x = 0$:

$$\partial_x T_e(0,t) = 0 \quad \text{and} \quad \partial_x T_l(0,t) = 0.$$

It was verified for each of the test cases that a computational domain of thickness reduced to L = 1000 μm (while the samples had a thickness of 2 mm) was sufficient to allow setting the following boundary conditions in $x = L$:

$$\partial_x T_e(L,t) = 0 \quad \text{and} \quad \partial_x T_l(L,t) = 0.$$

The initial conditions were set to

$$T_e(x,0) = T_l(x,0) = 300\,\text{K for } 0 \le x \le L.$$

The domain was meshed with uniform cells; it was verified that a cell size of 1nm was sufficient to reach convergence in mesh. The time step was set to 0.0001ps to satisfy a convergence criteria of 10^{-6} (residual in L^2 norm).

The electron and lattice temperatures calculated as functions of time in $x = 0$ for the different combinations of sub-pulses *n* and time between sub-pulses *Δt* are plotted in Figs. 2-3. The laser source power density is also drawn in the same plots.

Optics EXPRESS

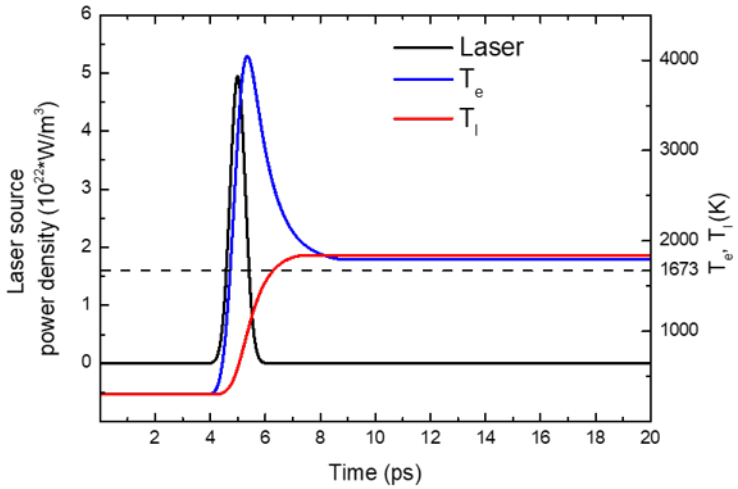

Fig. 2. Laser source power density, electron and lattice temperature as functions of time calculated on the top surface of the sample (i.e. in x = 0), in NPM. The black curve represents the laser power density. The dashed line corresponds to the melting temperature of stainless steel.

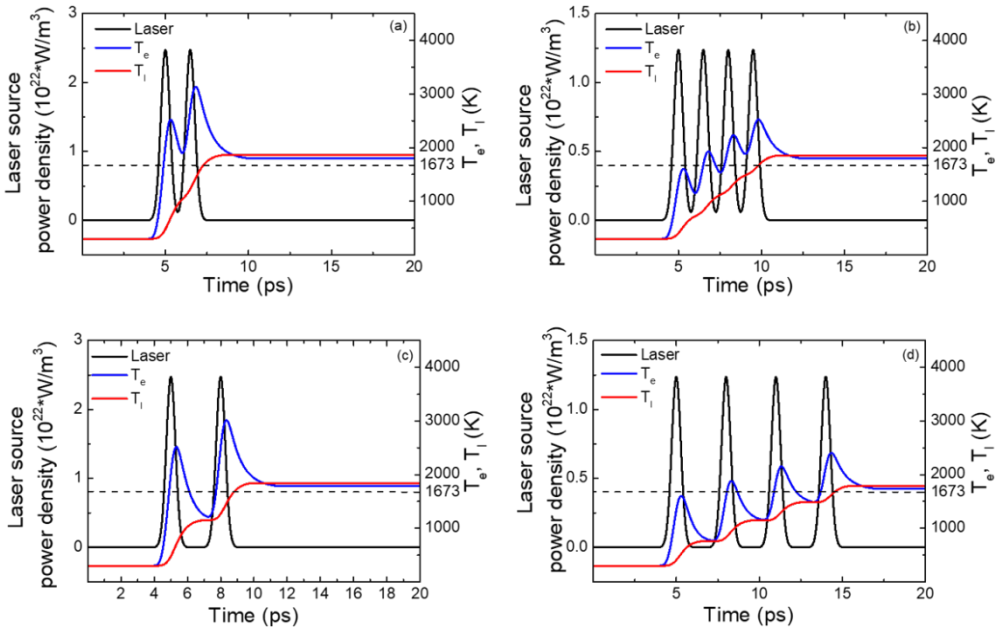

Fig. 3. Laser source power density, electron and lattice temperature as functions of time calculated on the top surface of the sample (i.e. in x = 0), in BM. (a) n = 2 and Δt = 1.5ps; (b) n = 4 and Δt = 1.5ps; (c) n = 2 and Δt = 3ps; (d) n = 4 and Δt = 3ps. The dashed line in each plot corresponds to the melting temperature of stainless steel.

It can be observed in Fig. 2 that in NPM the lattice reaches the melting temperature T_m after the laser is over (i.e. after the trailing tail of the laser pulse). On the contrary, it can be seen in Fig. 3 that in case of BM melting is achieved before the irradiation stops (i.e. before the burst is over). Therefore, it can be concluded that less energy is needed in BM for

Optics EXPRESS

reaching T_m. This indicates that using bursts of sub-pulses with ps delays enables a more efficient transfer of the laser energy to the material. This is better depicted in Fig. 4, where the normalized laser energy E_m needed to reach melting of the lattice is plotted as a function of the burst features.

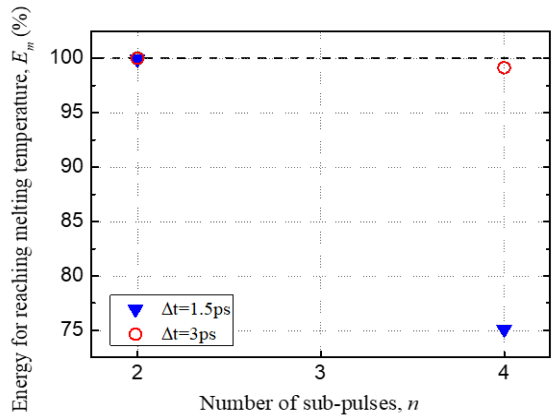

Fig. 4. Normalized energy for reaching melting versus number of sub-pulses, for Δt = 1.5ps and Δt = 3ps. For comparison, the dashed line represents the NPM case, where all the laser energy is needed to reach melting.

According to the simulation results, in NPM the entire amount of the laser energy absorbed by the sample is needed for melting to take place. The same occurs in BM with n = 2 and Δt = 3ps. However, as the pulse splitting increases from 2 to 4, less energy E_m is required for reaching melting. Results of this analysis are summarized in Tab. 2.

Table 2. Normalized energy needed for reaching the melting temperature in NPM (i.e. *n* = 1) and BM.

n \ *Δt*	1.5 ps	3 ps
1	100%	100%
2	99.9%	100%
4	75.0%	99.1%

4.2 Ablation thresholds

The threshold fluence F_{th} in case of NPM and BM has been estimated by using the method proposed by Liu [44], which assumes a Gaussian profile for the spatial energy distribution of the laser beam, and is based on the following equation:

$$D^2 = 2w^2 \ln\left(\frac{F_0}{F_{th}}\right), \tag{7}$$

where D is the crater diameter, and w the laser spot radius on the sample surface. F_0 is the peak laser fluence given by

$$F_0 = \frac{2E}{\pi w^2}, \tag{8}$$

where E is the energy of the undivided pulses E_p in NPM, while in BM it indicates the sub-pulse energy E_{sp}.

Optics EXPRESS

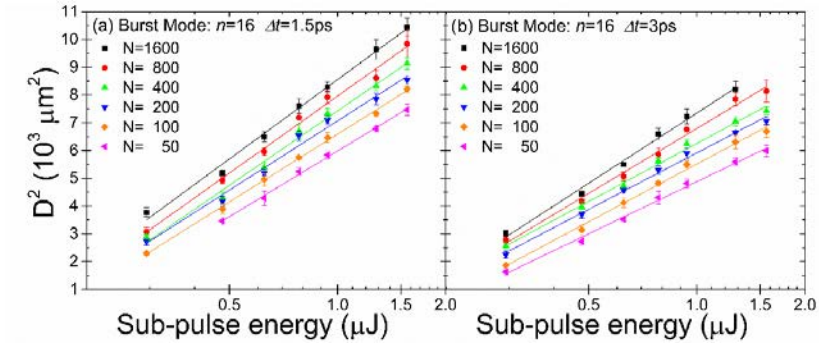

Fig. 5. Semi-log plot of squared diameters versus sub-pulse energy for n = 16 sub-pulses in the bursts with a time separation of (a) 1.5 ps and (b) 3 ps, for stainless steel when irradiated with N = 50, 100, 200, 400, 800, 1600 bursts.

The fits plotted in Fig. 5 show a linear dependence for each value of investigated *N*. This trend is confirmed for all the combinations of explored parameters reported in Table 1. Furthermore, the fitting lines are almost parallel, thus indicating that uniform focusing conditions were kept during the experiments. Therefore, the beam spot size on the target surface was determined from the slope of the linear fit, based on Eq. (7). The resultant average value of the laser spot radius is 43.1 ± 3.8 μm. This procedure for determining the beam spot size is based on the hypothesis that the ablated diameter is only a function of the beam energy profile because the pulse duration in the ultrashort regime implies negligible heat diffusion.

The threshold fluence was estimated from the intersection of the linear fits with the x-axis. Figure 6 shows the trend of the threshold fluence as a function of the total number of sub-pulses, $N_{tot} = N{\cdot}n$, for the two different time separations. The threshold fluence measured in case of NPM (black squares) is also reported for comparison. A decrease of the threshold fluence is clearly observed as the total number of impinging sub-pulses N_{tot} increases. This result is in agreement with other literature data and is ascribed to incubation [24,26–31].

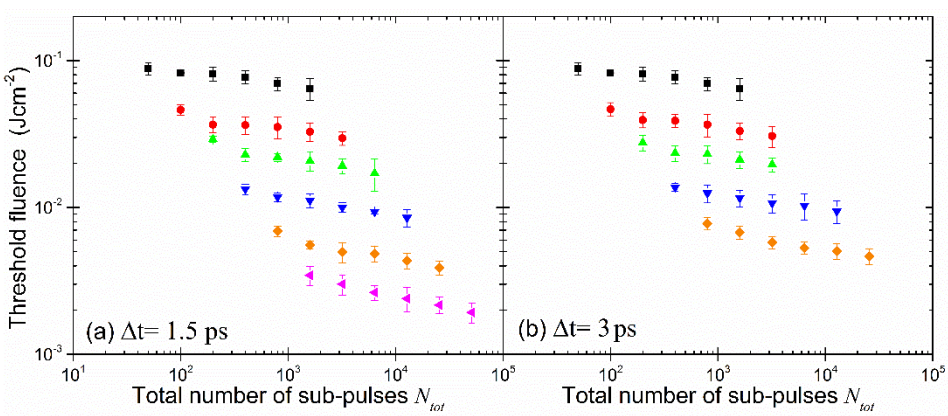

Fig. 6. Bi-log plot of threshold fluence as a function of the total number of sub-pulses Ntot = N·n. The time separation between consecutive sub-pulses in the burst is (a) 1.5 ps and (b) 3 ps. ● n = 2, ▲ n = 4, ▼ n = 8, ◆ n = 16, ◀ n = 32. ■ NPM.

In Fig. 6 it is evident that the decrease of damage threshold in BM is mainly due to the growth of the number of sub-pulses constituting the burst, rather than the number of bursts itself. In fact, for Δt = 1.5 ps a threshold reduction of 93% was found when increasing N_{tot} from 100 to 1600, while keeping the same number of bursts N = 50 and just changing the number of sub-pulses per burst from 2 to 32. Similarly, 83% reduction of the threshold

Optics EXPRESS

fluence was observed for Δt = 3 ps and N = 50, when increasing the number of sub-pulses from 2 to 16, and thus increasing N_{tot} from 100 to 800. On the other hand, the threshold fluence shows a slower decrease when increasing the number of bursts N and keeping the same number of sub-pulses n. This can be observed in e.g. the cases of Δt = 1.5 ps, n = 2, and N from 50 to 800 and Δt = 3 ps, n = 2 and N from 50 to 400. In both of these cases, the measured reduction of the threshold fluence was 28%.

A further characteristic result emerging from the analysis of the experimental data obtained in BM is that for a fixed total number of sub-pulses N_{tot} different damage threshold values were found for each combination of N and n. This is better highlighted in Table 3 summarizing data for N_{tot} = 1600. The literature models introduced to interpret incubation effect in NPM do not take into account this behavior since they all return one single value of threshold fluence once the number of impinging pulses is fixed [24,26,31–33].

Table 3. Threshold fluences for the combinations of *N* and *n* giving N_{tot} = 1600.

Number of bursts N	Sub-pulses in the burst n	Total number of sub-pulses $N\ tot$	Threshold fluence F_{th} [Jcm^{-2}] Δt =1.5 ps	Δt =3 ps
800	2		0.0328	0.0332
400	4		0.0207	0.0211
200	8	1600	0.0111	0.0116
100	16		0.0056	0.0067
50	32		0.0034	

4.3 Incubation

In order to directly compare BM and NPM and to investigate the influence of burst features on the incubation behavior, the Jee's model [24] has been extended to fit also experimental data of BM processing. In that aim, a dependence of the incubation coefficient S on the characteristics of the bursts is here introduced:

$$F_{th,b}(N) = F_{th,b}(1) \cdot N^{(S_n - 1)}, \tag{9}$$

where $F_{th,b}(N)$ represents the threshold fluence with N bursts, while $F_{th,b}(1)$ is the threshold fluence for a single burst. It is worth noticing that Eq. (9) represents also the case of NPM when n = 1.

The incubation coefficient S_n for each investigated values of n and Δt was obtained and its dependence from n is shown in Fig. 7. The value of the incubation coefficient obtained in NPM is also reported for comparison.

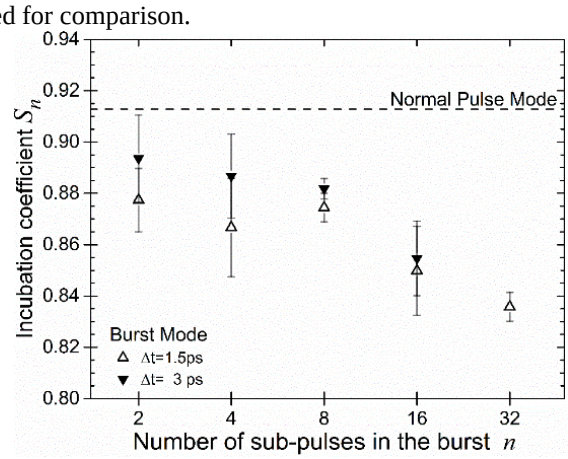

Fig. 7. Incubation coefficient Sn versus the number n of sub-pulses in the burst for the two different time separations, 1.5 and 3 ps. The dashed line represents the incubation coefficient in case of Normal Pulse Mode.

Optics EXPRESS

It can be observed that the BM incubation coefficient S_n noticeably decreases with the number of sub-pulses in the burst, thus revealing that the higher the pulse splitting, the stronger is the incubation effect, independent of the time separations. The NPM incubation coefficient, which is equal to 0.91, is in very good agreement with values reported by Di Niso and Mannion [26,31]. It can also be seen that the NPM incubation coefficient is always higher than in BM, thus indicating that the use of bursts enhances the incubation effect. The origin of the increased incubation observed when using bursts of pulses can be of different nature, like e.g. damage accumulation that weakens the molecular bonding, changes in the surface chemistry and/or topography. All these mechanisms may contribute to the lowering of the damage threshold and/or to the variation of the absorption length, so that the deposited energy is increased during multi-burst laser irradiation [45]. Results of numerical solutions of TTM presented in section 3, indeed highlight that the laser energy input needed to reach the melting temperature is lower in BM than in NPM and it tends to diminish as the pulse splitting increases (as it is shown in Table 2 from $n = 2$ to $n = 4$).

In Fig. 7 a dependence of BM incubation coefficient on the separation time between sub-pulses can also be noticed. In particular, with a shorter intra-burst delay of 1.5 ps we obtained lower incubation coefficient values compared to 3 ps. Since from the numerical simuliations it was shown that the shorter the time separation, the smaller the laser energy needed for the lattice to reach the melting temperature, it can be argued that such a different rate of energy deposition has an influence on incubation.

Although results of the numerical simulations are limited to single bursts with maximum pulse splitting of 4 sub-pulses, they indicate a clear trend which is expected to be enhanced in case of multi-burst irradiation and higher pulse splitting.

5. Conclusion

An experimental study on the laser ablation threshold fluence using bursts of 650-fs ultrashort pulses at repetition rate of 100 kHz and 1030 nm have been conducted on stainless steel targets. The number n of sub-pulses in the bursts was varied from 2 up to 32 while the intra-burst delay was 1.5 ps or 3 ps. For comparison, analogous experiments have been carried out with undivided pulses (Normal Pulse Mode) in the same experimental conditions.

For both processing modes, it was found that the threshold fluence decreases when increasing the total number of sub-pulses. In particular, in NPM the trend of threshold fluence F_{th} versus the number of undivided pulses N was fairly well described by the Jee's model. It resulted in an estimated value of the incubation coefficient $S = 0.91$ that is in good agreement with the literature [26,31]. In case of BM processing, for a given total number N_{tot} of impinging sub-pulses different values of the threshold fluence were found depending on the burst features, i.e. the combinations of N and n resulting in the same value of N_{tot}. Such a result cannot be explained with any of the existing incubation models developed for NPM.

Therefore, the existing model was extended also to BM by introducing an incubation coefficient S_n which takes into account the burst features, i.e. the number of sub-pulses in the bursts. Such model was found to fit the experimental data in all the investigated conditions. It was found that in BM the incubation factors S_n are always lower than the corresponding coefficient S obtained in NPM. A significant decrease of S_n is observed with the number of sub-pulses n in the burst, independently of the intra-burst time separation, thus indicating an enhancement of incubation with the pulse splitting. This behavior can be explained in terms of different concurring mechanisms, like e.g. damage accumulation or change in surface chemistry and topography, which result in a more efficient deposition of the laser energy into the material when bursts with a high number of sub-pulses are used. Results of numerical simulations calculating the temporal and spatial evolution of the electron and lattice temperature during ultrafast laser irradiation with single pulse or burst showed that the portion of absorbed laser energy needed for the lattice to reach the melting temperature

Optics EXPRESS

decreases as *n* increases. Such effect is expected to be even more pronounced in case of multi-pulse/burst irradiation.

It was further experimentally observed that the intra-burst time delay influences the incubation effect. In fact, a lower incubation coefficient was found for 1.5 ps time separation between sub-pulses compared to the 3 ps case. According to the numerical results, the longer the time separation the higher is the laser energy input needed to reach melting. Therefore, it can be argued that the rate of energy deposition, which depends on the burst features, influences incubation.

A deeper understanding of the physical mechanisms behind the increased incubation observed with BM processing, can be achieved by further investigating the surface chemistry of the irradiated area and refining the model by taking into account changes of the optical properties of the material with a phase close or in the melting region, which was beyond the scope of the present paper.